Surgery Open Science 6 (2021) 21–28

Contents lists available at ScienceDirect

Surgery Open Science

journal homepage: https://www.journals.elsevier.com/surgery-open-science

In vivo diffuse reflectance spectroscopic analysis of fatty liver with inflammation in mice

Yasuhiro Takihata, MD [a,b], Satoko Kawauchi, PhD [b,*], Sho Ogata, MD, PhD [c], Izumi Nishidate, PhD [d], Shunichi Sato, PhD [b], Junji Yamamoto, MD, PhD [a,1], Yoji Kishi, MD, PhD [a]

[a] Department of Surgery, National Defense Medical College, 3-2 Namiki, Tokorozawa, Saitama 359-8513, Japan
[b] Division of Bioinformation and Therapeutic Systems, National Defense Medical College Research Institute, 3-2 Namiki, Tokorozawa, Saitama 359-8513, Japan
[c] Department of Pathology and Laboratory Medicine, National Defense Medical College Hospital, 3-2 Namiki, Tokorozawa, Saitama 359-8513, Japan
[d] Graduate School of Bio-Applications & Systems Engineering, Tokyo University of Agriculture and Technology, 2-24-16 Naka-cho, Koganei, Tokyo 184-8588, Japan

ARTICLE INFO

Article history:
Received 26 March 2021
Received in revised form 13 June 2021
Accepted 1 July 2021
Available online 24 July 2021

ABSTRACT

Background: Nonalcoholic steatohepatitis is a progressive liver disease that can lead to cirrhosis, hepatocellular carcinoma, and hepatic failure. Thus, the diagnosis of nonalcoholic steatohepatitis, especially discrimination from nonalcoholic fatty liver, is crucial, but reliable methods other than invasive biopsy have not been established yet. In this study, we investigated the usefulness of diffuse reflectance spectroscopy, which does not require tissue collection, to evaluate the pathological states of fatty liver with inflammation.

Materials and Methods: We performed in vivo optical fiber-based diffuse reflectance spectroscopy in both the near-infrared and visible spectral regions for livers in STAM mice, which typically show steatosis at 6 weeks, steatohepatitis at 8 weeks, and fibrosis at 12 weeks of age. After diffuse reflectance spectroscopy, all of the liver tissues were histologically analyzed and scored on the basis of the rodent nonalcoholic fatty liver disease scoring system. We examined correlations between the diffuse reflectance spectra and scores associated with steatosis and inflammation.

Results and Conclusion: The results showed that the second derivative values of reflectance at 1204 nm, the lipid absorption peak in the near-infrared region, were strongly correlated with steatosis scores ($r = 0.9172$, $P < .0001$, $n = 20$) and that the differences of the first derivative values of reflectance in the visible region (570 nm − 550 nm) that reflect hemoglobin deoxygenation were significantly correlated with inflammation scores ($r = 0.5260$, $P = .0172$, $n = 20$). These results suggest that our diffuse reflectance spectroscopy method is useful for diagnosis of the states of steatosis with inflammation in livers and hence nonalcoholic steatohepatitis.

INTRODUCTION

Nonalcoholic fatty liver disease (NAFLD) is a spectrum of liver disorders that range from nonalcoholic fatty liver (NAFL) to nonalcoholic steatohepatitis (NASH). Because NASH can lead to cirrhosis, hepatocellular carcinoma, and liver failure [1], it is of great clinical importance to discriminate between NAFL and NASH. Currently, ultrasonography-guided percutaneous liver biopsy is the gold standard for discrimination. Liver biopsy can also be performed through a transjugular or laparoscopic route [2]. Regardless of the method used, liver tissue collection is highly invasive, causing pain (30% to 50% of patients experience pain, usually around the biopsy site), serious bleeding (0.6% of patients), and even death (up to 0.1% of patients) [2]. Additional problems arise due to sampling errors, limited sample volumes, and subjective biopsy interpretation [2]. Thus, it is imperative to develop a minimally invasive, reliable method that can provide opportune diagnosis for patients who are at risk of developing chronic liver diseases.

In the past few decades, diffuse reflectance spectroscopy (DRS) has been extensively applied to tissue diagnosis without biopsy [3,4]. Because light reflected from tissue (diffuse reflectance) has information on light absorption and scattering properties of the tissue, the states of absorption chromophores and scatterers can be monitored by spectroscopic analysis of diffuse reflectance signals. DRS for absorption chromophores can provide information on the contents of oxygenated/deoxygenated hemoglobins, water, and lipids [5], whereas DRS for light scatterers can indicate microstructural and functional changes in

* Corresponding author at: 3-2 Namiki, Tokorozawa, Saitama 359-8513, Japan.
E-mail addresses: y_takihata@ndmc.ac.jp (Y. Takihata), satok-bits@ndmc.ac.jp (S. Kawauchi), sogata@ndmc.ac.jp (S. Ogata), inishi@cc.tuat.ac.jp (I. Nishidate), ssato-bits@ndmc.ac.jp (S. Sato), j-yamamoto@umin.ac.jp (J. Yamamoto), ykishi-3su@ndmc.ac.jp (Y. Kishi).
[1] Present address: Ibaraki Cancer Center, Ibaraki Prefectural Central Hospital, 6528 Koibuchi, Kasama, Ibaraki 309-1793, Japan

https://doi.org/10.1016/j.sopen.2021.07.002

tissue. Thus, DRS enables real-time tissue diagnosis without tissue collection. Moreover, DRS enables repeated measurements at different sites, thus reducing the number of sampling errors that would occur with conventional biopsies. Indeed, spectroscopic data provide an objective diagnosis. Thus, the DRS method has recently been applied to monitor lipid deposition in livers in vivo and ex vivo [6,7]. To the authors' best knowledge, however, few reports have dealt with diagnosis of fatty liver with inflammation by DRS in vivo.

In this study, we examined whether the states of liver involving both steatosis and inflammation could be detected by DRS. For that purpose, we used STAM mice, which typically show steatosis (NAFL model) at 6 weeks of age, steatohepatitis (NASH model) at 8 weeks of age, and fibrosis at 12 weeks of age [8]. For exposed livers of mice at each stage, we measured diffuse reflectance spectra both in the near-infrared (NIR) and visible (VIS) spectral regions to assess relative lipid content and hemoglobin oxygen saturation, respectively. We assumed that an influx of inflammatory cells leads to hypoxia (inflammatory hypoxia), reducing hemoglobin oxygen saturation in the liver. We carefully compared spectroscopic data with the results of histopathological analyses on the basis of the rodent NAFLD scoring system [9].

MATERIALS AND METHODS

All of the procedures used in the animal experiments in this study were approved by the Committee on Animal Ethics at the National Defense Medical College, Japan (permission numbers 12093 and 18101).

Animals. STAM mice of 5 and 10 weeks of age were obtained from Stelic Institute & Co (Tokyo, Japan). STAM mice were obtained by treating C57BL/6J male mice with a single subcutaneous injection of 200 μg streptozocin (Sigma, MO, USA) at 2 days after birth and feeding with High Fat Diet 32 (CLEA Japan, Tokyo, Japan). To induce different stages of NAFLD, the mice received the high-fat diet for 6, 8, and 12 weeks to induce steatosis, steatohepatitis, and fibrosis, respectively. Control mice (C57BL/6J male mice of 8 weeks of age) were purchased from Japan SLC, Inc (Shizuoka, Japan). We used male mice because STAM mice have been established only for males. All of the animals were caged in animal rooms and had free access to food and water for the duration of experiments.

Instrumentation for DRS. Figure 1 shows schematics for in vivo DRS of mice livers. The DRS system consisted of a tungsten-halogen lamp (400–1700 nm; BPS2.0; B&W Tek, Inc., Newark, DE, USA), a NIR spectrometer (900–1700 nm; TG-NIR C9406GC; Hamamatsu Photonics, Inc., Hamamatsu, Japan), a VIS spectrometer (200–900 nm; USB4000; Ocean Optics, Inc., Dunedin, FL, USA), and a pair of optical fibers (a source fiber and a detection fiber) with a core diameter of 600 μm. Light from the lamp was collimated and power-adjusted and then coupled to one end of the source fiber, and the other end was placed on the liver surface. For light power adjustment, a variable neutral density (ND) filter was used to set the irradiation power for the liver at 350 and 100 μW for NIR DRS and VIS DRS, respectively. A long-wavelength-absorbing filter was used to cut light of wavelengths longer than 1000 nm for VIS DRS. For the detection fiber, one end was connected to either of the spectrometers, and the other end was placed on the liver surface. The center-to-center distance of 2 fibers was kept constant at 1 mm on the liver. Light transmitted through the source fiber penetrated into the liver, and diffuse reflectance was captured with a detection fiber and delivered to the spectrometer. The integration times were set to be 1000 ms for NIR DRS and 400 ms for VIS DRS.

In Vivo DRS. STAM mice and control mice were anesthetized by intraperitoneal injection of pentobarbital sodium (20 mg/kg animal weight). Mice were placed on a temperature-controlled body mat (37°C) in a supine position, and laparotomy was performed to expose the liver. End faces of a pair of optical fibers described above were placed on the liver surface of the median lobe. In one measurement for each liver, DRS spectra were measured twice using the setup shown in Fig 1 in a darkened room, and 2 sets of obtained spectral data were averaged. This procedure was conducted by the same operator (Y.T.) to ensure constant fiber contact conditions on the liver surface. After conducting DRS, mice were sacrificed, and hepatectomy was performed to obtain tissue for measurement. Histological analysis of the tissues was performed as described below.

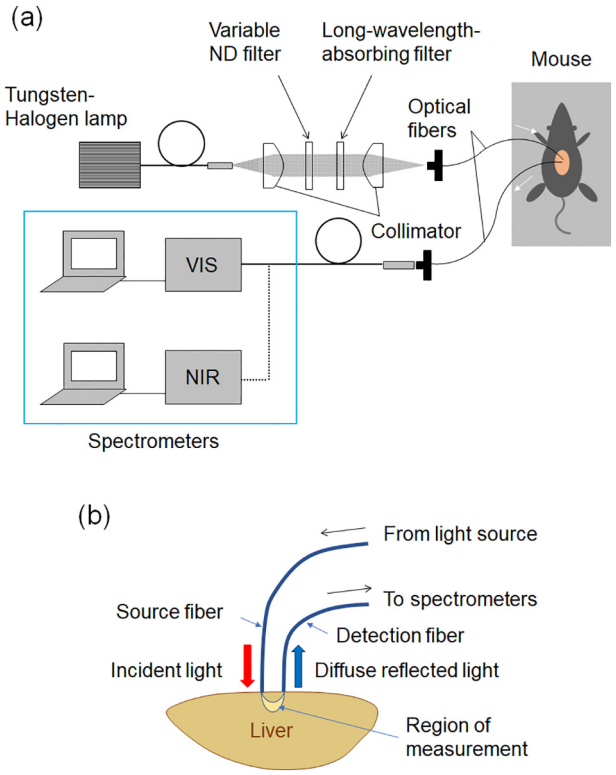

Fig 1. (a) Diagram of the setup for diffuse reflectance spectroscopy (DRS) of the mouse liver. A long-wavelength-absorbing filter was used only when a VIS spectrometer was used. (b) Conceptual sketch of DRS. ND: neutral density; VIS: visible; NIR: near-infrared.

Data Analysis. Diffuse reflectance spectra were acquired for 5 livers in each group of mice. For data processing, the background (dark) spectrum was subtracted from the measured spectrum using supplied software. A reference reflectance spectrum was also measured with a certified diffuse reflectance standard plate (SRS-99-020; Labsphere, Inc., North Sutton, NH, USA), for which the fiber probe ends were positioned near the plate in a noncontact manner. Measured diffuse reflectance spectra were converted to relative reflectance values using the following equation:

$$R_d(\lambda) = \frac{S(\lambda) - D(\lambda)}{S_{ref}(\lambda) - D(\lambda)}, \quad (1)$$

where $R_d(\lambda)$ is the relative reflectance intensity at the wavelength λ, $S(\lambda)$ is the diffuse reflectance intensity for the liver at the wavelength λ, $D(\lambda)$ is the dark intensity at the wavelength λ, and $S_{ref}(\lambda)$ is the reference signal intensity from the reflectance standard at the wavelength λ.

To assess the relative lipid content and tissue (hemoglobin) oxygen saturation, the relative reflectance spectra (R_d) obtained by Eq. (1) were analyzed on the basis of the second- and first-derivative values, respectively [10]. The principal advantage of using the first-derivative spectra is that the effects of background absorbance and scattering that are less dependent on wavelength can be eliminated. However, there are cases when an absorption peak of interest is significantly overlapped by

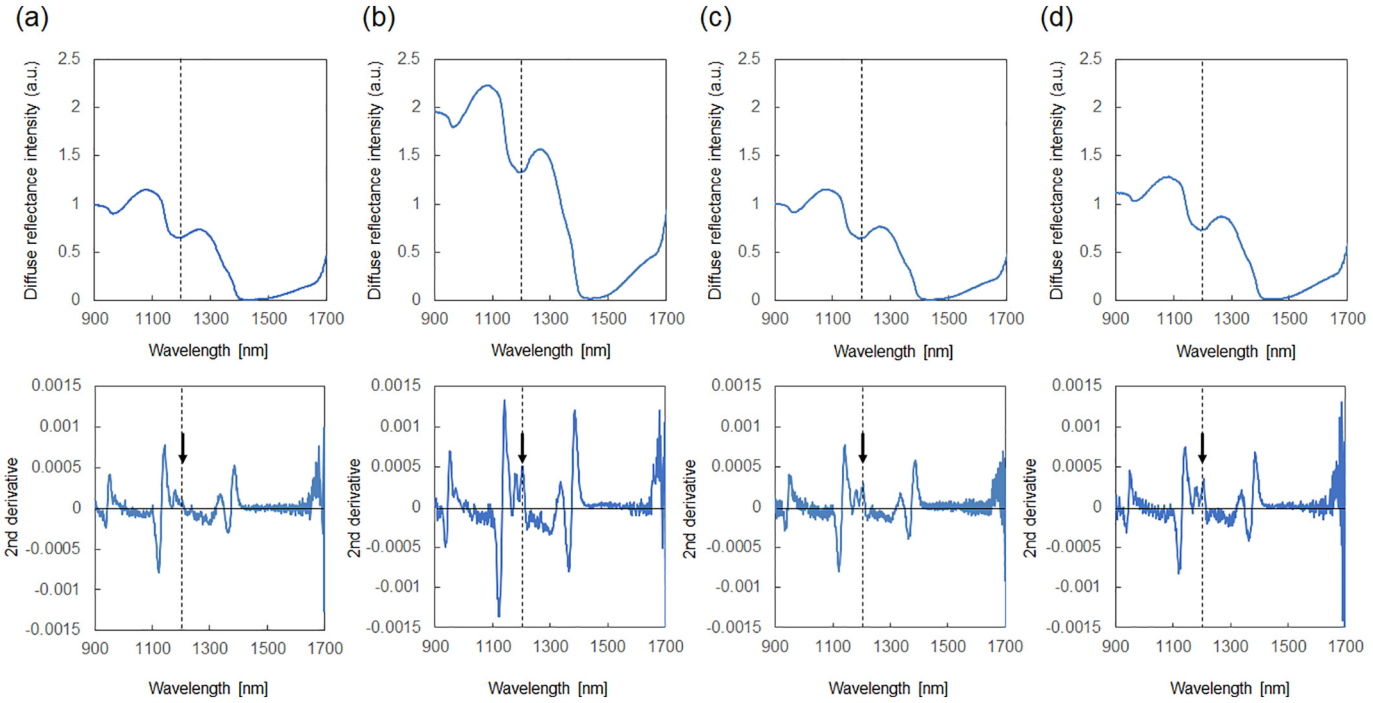

Fig 2. Averaged raw diffuse reflectance spectra (upper row) and their second-derivative values (lower row) in the NIR region for each group of mice ($n = 5$). (a) Control mice of 8 weeks of age. STAM mice of (b) 6 weeks, (c) 8 weeks, and (d) 12 weeks of age. The vertical dashed line and arrow indicate the peak absorption wavelength of lipid (1204 nm) and the second-derivative signal of interest, respectively.

other absorption peaks. In such cases, the first derivative is unreliable in detecting changes in the absorption peak of interest. However, if there is a certain difference between the spectral curvature of the chromophore of interest and spectral curvatures of other chromophores, the second derivative is able to detect changes in the absorption peak of interest [11]. The detection of change in the absorption peak of lipids (1204 nm) that is overlapped by the broader absorption peak of water (1200 nm) corresponds to this case [12]. Thus, we used the second-derivative values to evaluate the relative lipid content in the liver tissue. In the VIS spectral region, oxygenated and deoxygenated hemoglobins are the dominant chromophores, and their absorption coefficients differ depending on the wavelength. Thus, the first-derivative spectra of liver tissue depend on hemoglobin oxygen saturation. In this study, we used the difference of the first-derivative value at 570 nm and that at 550 nm (570 nm − 550 nm) to evaluate relative changes in tissue hemoglobin oxygen saturation on the basis of the assumption of inflammation-induced local hypoxia described above.

Histological Analysis. Sectioned tissue was fixed in 10% formalin, embedded in paraffin, and subjected to hematoxylin and eosin (H&E) staining. An expert pathologist (S.O.) blindly analyzed histological images of all of the liver samples on the basis of rodent NAFLD scoring system [9]. For each liver sample, three representative images from a region where DRS was performed were obtained, and proportions of areas showing specific histological features, i.e., macrovesicular steatosis, microvesicular steatosis, and hepatocytic hypertrophy, to the whole areas of images were separately estimated and scored as 0 (<5%), 1 (5%–33%), 2 (34%–66%), or 3 (>66%) points. The steatosis score was defined as the summation of scores for macrovesicular steatosis, microvesicular steatosis, and hepatocytic hypertrophy. For assessing inflammation status, the number of inflammatory focus (i.e., an aggregate of several or more inflammatory cells) per high-power field was counted and scored as 0 (<0.5 focus), 1 (0.5–1.0), 2 (1.0–2.0), or 3 (>2.0) points (inflammation score). The liver was diagnosed as NASH when both the steatosis score and the inflammation score were equal to or higher than 1 [9].

Statistical Analysis. We used the Shapiro–Wilk test to check the normality of data for each group of mice, i.e., the second-derivative values of the reflectance spectra at 1204 nm ($n = 5$), difference in the first-derivative values of reflectance spectra (570 nm − 550 nm) ($n = 5$), histological steatosis scores ($n = 5$), and histological inflammation scores ($n = 5$). Statistical differences were determined for data of different mice groups using the nonparametric Wilcoxon test. Spearman correlation test was used to examine the correlation between the second-derivative values of reflectance spectra at 1204 nm and histological steatosis scores and the correlation between the difference of the first-derivative values of reflectance spectra (570 nm − 550 nm) and histological inflammation scores. All of the statistical analyses were conducted using JMP 14 statistical software (SAS Institute Inc., USA).

RESULTS

Diffuse Reflectance Spectra. Figure 2 shows averaged ($n = 5$) raw diffuse reflectance spectra (upper row) and their second derivative values (lower row) in the NIR region (900–1700 nm) for the livers of (a) control mice and STAM mice of (b) 6 weeks, (c) 8 weeks, and (d) 12 weeks of age. Raw diffuse reflectance spectra for 5 mice in each group are shown in Supplementary Fig 1. Two repeatedly measured spectra and their average, which was used to obtain a raw diffuse reflectance spectrum in a mouse of each group, are shown in Supplementary Fig 2 and indicate a high reproducibility. In Fig 2, the upper row shows reflection (not absorption) spectra and valleys, which correspond to the absorption peaks of some chromophores. Three valleys centered at ~980 nm, ~1190 nm, and ~1400 nm, which are commonly observed, correspond to water absorption peaks [13]. A sign of the chromophore of interest, i.e., lipid, is not clear at 1204 nm. The spectral shapes are similar for all groups of mice, but reflectance intensity for 6-week-old STAM mice is higher

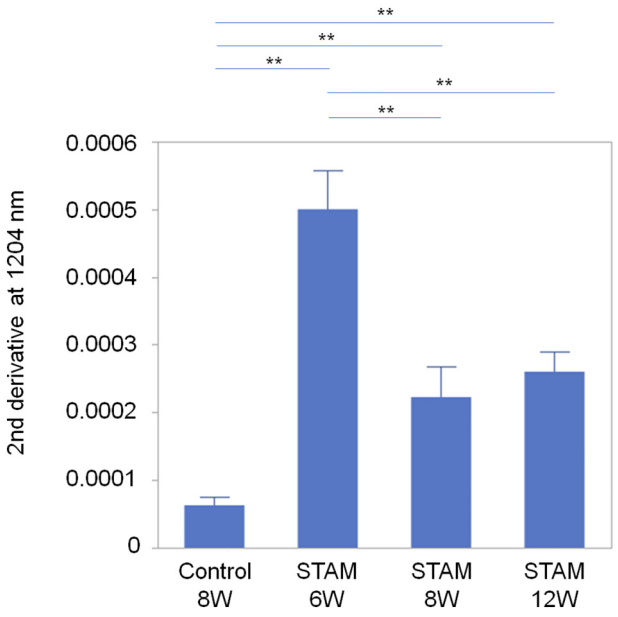

Fig 3. Second-derivative values at 1204 nm for each group of mice. *$P < .05$, **$P < .01$.

as a whole than intensities for other groups of mice. As described later in histological analysis, lipid content in the liver was highest for 6-week-old STAM mice, and lipid has a high scattering coefficient [14], increasing diffuse reflection. In addition, a higher content of lipid means a reduced content of water, which is the dominant chromophore in the tissue, decreasing the light absorption of water and hence increasing diffuse reflection. These 2 factors are the reasons for the highest reflection intensity for the liver in 6-week-old STAM mice. Three sharp biphasic peaks seen in the second-derivative spectra (lower row in Fig 2) correspond to the water absorption peaks described above. In the livers of all groups of STAM mice, smaller but clear double peaks are seen at 1180 and 1204 nm, which are attributable to absorptions due to cholesterol and lipid [15], respectively. As described above, we used the second-derivative values (mean ± SEM) at 1204 nm to evaluate relative lipid content in the liver (Fig 3). The mean values for all of the 3 groups of STAM mice were significantly higher than that for control mice ($P < .01$). The livers of 6-week-old STAM mice showed the highest value of 0.00050 ± 0.00006; there were significant differences between the value for 6-week-old STAM mice and the values for all other groups of STAM mice ($P < .01$), indicating the highest lipid content in the livers of 6-week-old STAM mice.

Figure 4 shows averaged ($n = 5$) raw diffuse reflectance spectra (upper row) and their first derivatives (lower row) in the VIS region (500–600 nm) for the livers of (a) control mice and STAM mice of (b) 6 weeks, (c) 8 weeks, and (d) 12 weeks of age. Raw diffuse reflectance spectra for 5 mice in each group are shown in Supplementary Fig 3. Two repeatedly measured spectra and their average, which was used to obtain a raw diffuse reflectance spectrum in a mouse of each group, are shown in Supplementary Fig 4 and indicate high reproducibility. In the raw spectra (upper row) in Fig 4, a single broad valley centered at ~555 nm is commonly seen, and it corresponds to the broad absorption peak due to deoxyhemoglobin. The spectral shape of the valley bottom becomes slightly sharper when the level of tissue deoxygenation increases. Change in the deoxygenation level is more clearly seen in the first-derivative spectra (lower row). At the absorption peak wavelength for deoxyhemoglobin of ~555 nm, the first-derivative value changes from minus to plus, and its slope theoretically becomes steeper with the higher deoxygenation level. Thus, the difference in the first-derivative values at 550 nm and at 570 nm (570 nm − 550 nm) can be used as an indicator of deoxygenation level (Fig 5). Because we assumed that inflammation caused hemoglobin deoxygenation, a higher value means a more intense inflammation in the livers. It was shown that the values for all three groups of STAM mice were higher than the value for control mice, although there was a significant difference in the value only between 8-week-old STAM mice (0.00310 ± 0.00099) and control mice (0.00024 ± 0.00153) ($P < .05$). This indicates that the livers of 8-week-old STAM mice were the most highly deoxygenated and the most highly inflamed among all groups of mice on the basis of our assumption.

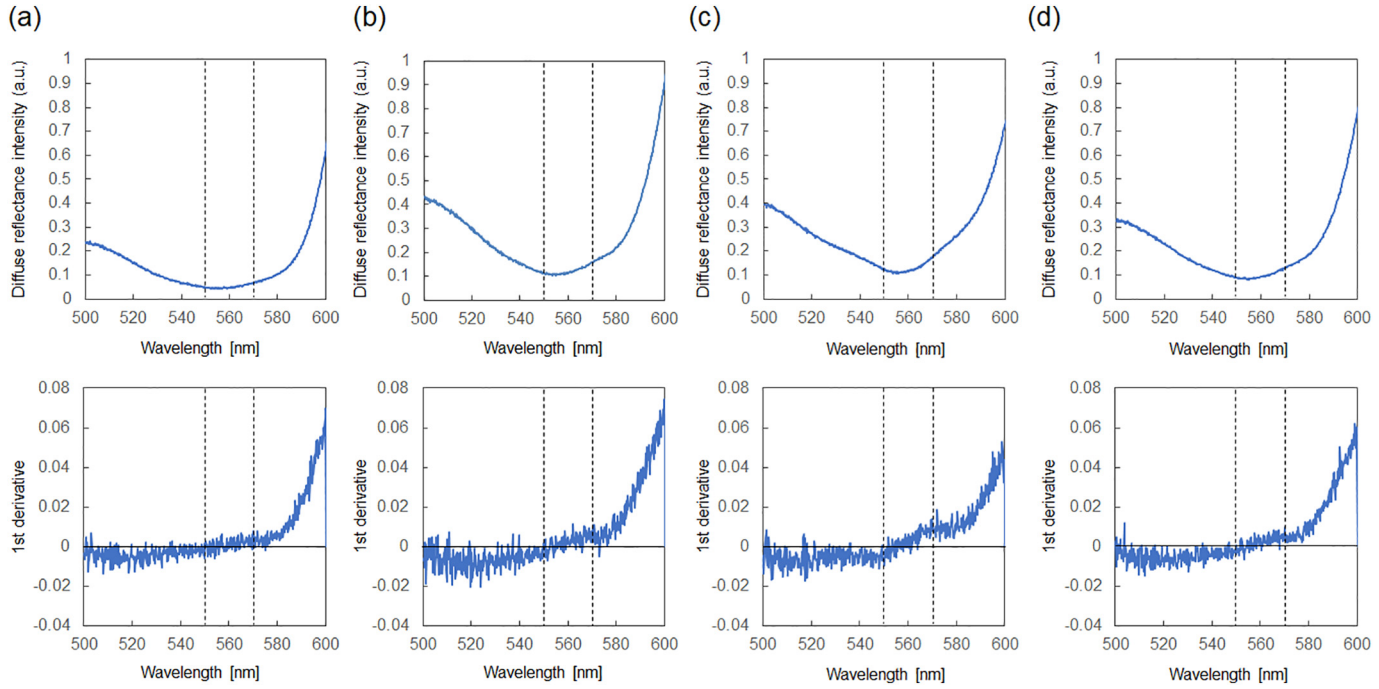

Fig 4. Averaged raw diffuse reflectance spectra (upper row) and their first derivatives (lower row) in the VIS region for each group of mice ($n = 5$). (a) Control mice of 8 weeks of age. STAM mice of (b) 6 weeks, (c) 8 weeks, and (d) 12 weeks of age. Vertical dashed lines indicate the wavelengths of 550 and 570 nm.

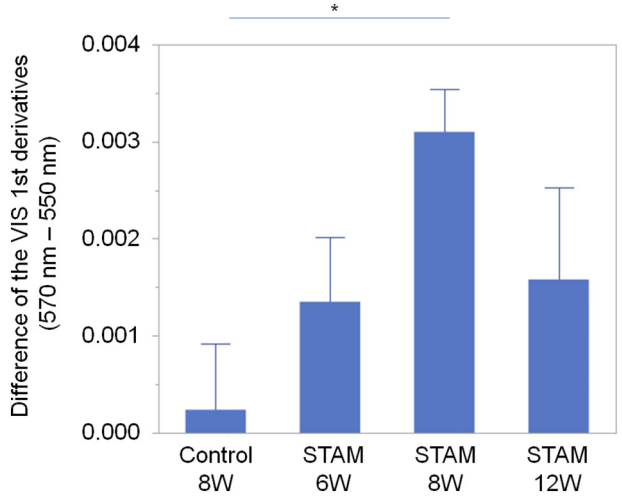

Fig 5. Difference of the first-derivative values at 550 and at 570 nm (570 nm − 550 nm) for each group of mice. $^{*}P < .05$, $^{**}P < .01$.

Histological Analysis. Figure 6 shows representative H&E-stained images of the livers of all groups of mice. In the liver of a 6-week-old STAM mouse (Fig 6, *b*), macrovesicular steatosis (dashed line arrow) and microvesicular steatosis (solid line arrow) are observed, while some hepatocytes swell (open arrow), indicating hepatocytic hypertrophy. Additional to these steatotic findings, unexpectedly, clusters of inflammatory cells are also seen (black line circle, Fig 6, *b*). Intense aggregation of inflammatory cells (black line circle) is seen in the liver of an 8-week-old STAM mouse (Fig 6, *c*), but the number of lipid droplets is much smaller than that in liver of the 6-week-old STAM mouse. The liver of a 12-week-old STAM mouse shows fibrosis (Fig 6, *d*); intracytoplasmic lipid droplets and lobular inflammatory focus are not evident.

Images for all groups of mice ($n = 5$ for each group) were scored on the basis of the rodent NAFLD scoring system. Figure 7 *a* and *b* shows steatosis scores and inflammation scores, respectively, for all groups of mice. Steatosis score was the highest for 6-week-old STAM mice; 6-week-old STAM mice showed statistically higher scores than those for 8-week-old STAM mice ($P < .05$). Inflammation scores for 6-week-old and 8-week-old STAM mice were significantly higher than the score for control mice ($P < .05$). The high inflammation score for 6-week-old STAM mice (nominally exhibiting NAFL, not NASH) was unexpected, but this is consistent with the results of histopathological examination (Fig 6, *b*).

Correlation Between DRS Parameters and Histopathological Scores. Figure 8, *a* shows the correlation between the NIR (1204 nm) second-derivative values and steatosis scores. The Spearman rank correlation coefficient was 0.9172 ($P < .0001$), indicating a strong correlation between these 2 parameters. Figure 8, *b* shows the correlation between the subtracted first-derivative values in the VIS region (570 nm − 550 nm) and inflammation scores. The Spearman rank correlation coefficient was 0.5260 ($P = .0172$), indicating a moderate correlation between these parameters. There was no significant correlation between the subtracted first-derivative values in the VIS region and steatosis scores or between the second-derivative values in the NIR region and inflammation (data not shown).

DISCUSSION

The objective of this study was to examine the feasibility of optical diagnosis, i.e., DRS, for states of steatosis with inflammation in the liver (NASH) in mouse models. For this purpose, both the lipid content and inflammation status must be determined for the liver. Whereas DRS was successfully applied to the diagnosis of fat deposition in the liver in some studies [16–18], no reliable methods have been reported for optical diagnosis of inflammation, to the authors' best knowledge. In this study, we used the second-derivative values at a lipid absorption peak of 1204 nm in the NIR region to assess relative lipid content in the liver and found a strong correlation between the values and histological steatosis scores (Fig 8, *a*). The use of the second-derivative values is considered to be effective for detecting the absorption signal of lipid, which overlaps that of water in the NIR region. For diagnosis of inflammation, we assumed that inflammation could cause oxygen demand outstripping oxygen supply, inducing local hypoxia (inflammatory hypoxia) [19] and hence deoxygenation of hemoglobin. Based on this assumption, we used the difference of the first-derivative values (570 nm − 550 nm) in the VIS region to evaluate hemoglobin oxygen saturation and found a moderate correlation between the values and histological inflammation scores. This seems to support our inflammation hypothesis for the liver. Overall, the results obtained in this study suggest that our DRS method is useful for monitoring lipid content as well as inflammation status in the liver, although further study is needed as described below.

When the present DRS method is compared with other noninvasive diagnostic modalities such as ultrasound-based vibration controlled transient elastography (VCTE) and magnetic resonance elastography (MRE), those elastography techniques implement liver stiffness measurements, enabling assessment of liver fibrosis [20,21]. It has been reported, however, that neither VCTE nor MRE can accurately predict NASH (independent of fibrosis) [22,23]. Although a recent advance in MRE technology (multifrequency 3-dimensional MRE) has shown the possibility of predicting NASH [24], no evidence-based correlation has yet been reported between the stiffness and biochemical/physiological property of NASH. Because our DRS method directly detects NASH using optical properties that relate to steatosis and inflammation in the liver, our method provides valuable information that significantly differs from the information obtained via VCTE or MRE.

STAM mice typically show steatosis (NAFL) in the liver at 6 weeks of age and steatohepatitis (NASH) in the liver at 8 weeks of age. For the

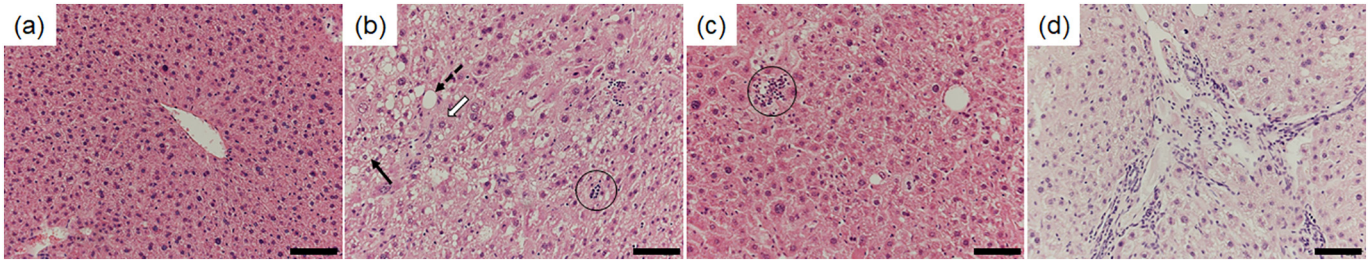

Fig 6. Representative images of hematoxylin and eosin (H&E)–stained liver sections from each group of mice (original magnification ×200). (a) Control mice at 8 weeks of age. STAM mice at (b) 6 weeks, (c) 8 weeks, and (d) 12 weeks of age. The black dashed line, solid line, and open arrows in panel b indicate a large lipid droplet (macrovesicular steatosis), a small lipid droplet (microvesicular steatosis), and hepatocellular hypertrophy, respectively. Black line circles in panels b and c indicate aggregation of inflammatory cells. Scale bar: 100 μm.

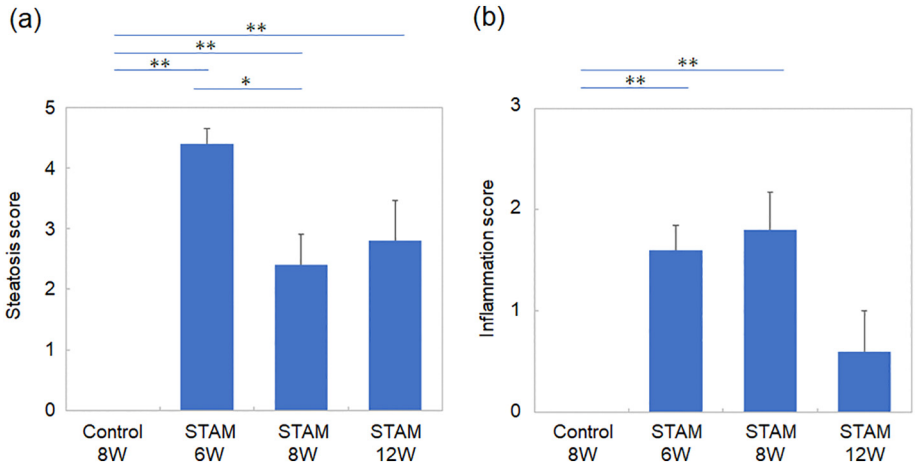

Fig 7. (a) Steatosis score and (b) inflammation score for each group of mice. $^{*}P < .05$, $^{**}P < .01$.

STAM mice used in this study, however, histological analyses showed a certain extent of inflammation even at 6 weeks of age (Figs 6, *b* and 7, *b*), whereas lipid content was clearly maximized at this age (Figs 6, *b* and 7, *a*) in the livers. Actually, a diagnosis of NASH was made for livers of both 6- and 8-week-old mice on the basis of the rodent NAFLD scoring system; livers of 6-week-old mice would probably be in the initial stage of NASH. According to the animal provider, inflammation can sometimes be observed at 6 weeks of age. Regardless of this fact, Fig 7, *b* shows that the STAM mice used in this study exhibited a wide range of inflammatory scores, i.e., from 0 to ~2. It can thus be said that the mice used in this study provided appropriate models for assessing inflammation status in the livers. It should be pointed out, however, that experiments using pure steatosis mice would be needed for further validation of our DRS method.

Although our DRS method was useful for diagnosing steatosis with inflammation, the reliability of the method for detection of inflammation should be improved because the correlation between optical deoxygenation signals and histological inflammation scores was moderate, not strong (Fig 8, *b*). For more comprehensive assessment of inflammation, the use of an additional optical signal might be useful. One possible candidate is absorption signals relating to the redox state of the mitochondrial respiratory chain (the redox state of heme aa_3 or CuA in cytochrome c oxidase) [25]. Hemoglobin-related signals may be affected by vascular density and distribution, whereas each single hepatocyte contains a few thousand mitochondria, providing uniform and sensitive signal sources for optical detection. The available data show that mitochondrial dysfunction would be a relevant event in the promotion of liver injury in the fatty liver and potentially responsible for the disease progression from simple steatosis to NASH [26].

In our DRS method, optical fibers need not to be inserted into liver tissue, enabling minimally invasive diagnosis. The observation depth for tissue analysis using the present DRS system is estimated to be a few hundreds of micrometers in the visible region and ~1 mm in the NIR region [27–29]. However, observation tissue depth can be controlled by changing the fiber-to-fiber distance, although the depth and the signal-to-noise ratio are in a tradeoff relation. Such a function of depth controllability would be useful for intraoperative diagnosis of the liver. In the present system, we used optical fibers with a core diameter of 600 μm, but their diameters can be reduced by optimization of the light source and detection conditions. By using a pair of thinner fibers that can be placed within a needle, clinical percutaneous diagnosis of the liver will be achieved without tissue collection (optical biopsy), in which the needle will be used to guide the fibers through the skin without puncturing the liver. For example, a pair of optical fibers with a core diameter of ~200 μm with a center-to-center distance of ~500 μm could be easily inserted through a conventional 16-gauge needle. To avoid unexpected liver puncture, an indwelling needle with a soft plastic catheter, through which fibers can be inserted, would be useful, ensuring noninvasive optical biopsy for the liver. When a deeper tissue diagnosis is needed in the liver, a transjugular route might be useful for fiber probe insertion. Tissue collection is not needed in this case also, which allows for a minimally invasive diagnosis. In the current system, NIR and VIS spectrometers are used for detection of lipid and inflammation (hemoglobin deoxygenation), respectively. However, hemoglobins

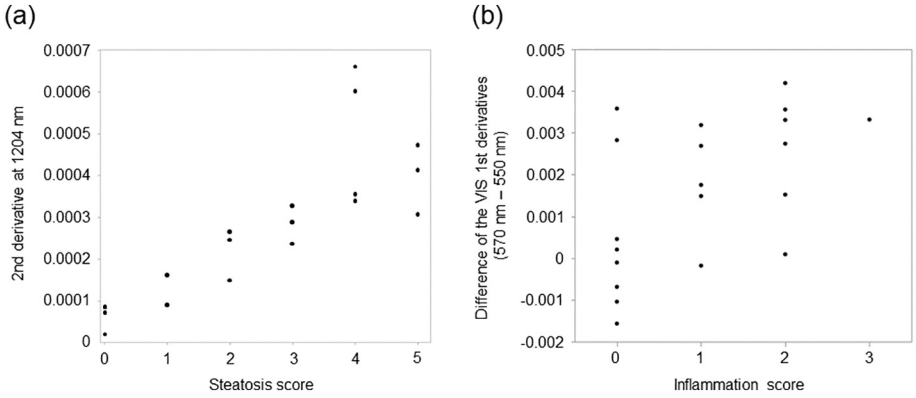

Fig 8. (a) Correlation between the second-derivative values at 1204 nm and steatosis scores. Spearman correlation = 0.9172 ($P < .0001$). (b) Correlation between the first-derivative values (570 nm − 550 nm) and inflammation scores. Spearman correlation = 0.5260 ($P = .0172$).

show a lower level but certain absorption in the NIR region, and their deoxygenation can therefore be monitored by using NIR reflectance signals. This enables simultaneous detection of steatosis and inflammation by using a single (NIR) spectrometer, which can simplify and downsize the system.

Although the present method would be technically applicable to humans as described above, a correlation should be considered between mouse liver and human liver for assessing the validity of our method. Importantly, it has been shown that the histological phenotype of a STAM NASH model developing steatosis, steatohepatitis, and fibrosis in the liver is similar to that of human clinical samples [30]. Furthermore, a recent comprehensive analysis has demonstrated a high correlation between the STAM mouse liver and human liver on genomic, transcriptomic, and lipidomic levels [30,31]. At least 15 test substances that showed the efficacies based on the pharmacological studies using STAM mice have been used in clinical studies treating NASH [32–34]. Taken together, these facts support the transferability of our in vivo method to clinical application.

Our next steps for further validation of our method include the following 3 issues. First, we will optimize our method to detect inflammatory hypoxia by quantifying tissue oxygen saturation levels instead of using first-derivative values because quantified values are more objective and reliable. Second, we will introduce an additional DRS signal relating to mitochondrial dysfunction (redox states of electron transport chain) [25], which will improve the detectability of cellular hypoxia, as described above. Third, we will incorporate ballooning injury in our diagnosis. Although ballooning degeneration is a key pathological feature of human NASH [35], conventional mouse models do not reproduce ballooning injury in their livers [9]; however, STAM mice can develop liver-ballooning degeneration [30]. Thus, the optical detection of liver-ballooning degeneration in STAM mice will further improve the usefulness and significance of our method, for which DRS signals relating to the above-mentioned mitochondrial dysfunction and light scattering reflecting cellular/subcellular morphological features can be used [36].

In conclusion, we showed that lipid and inflammation in the livers of STAM mice could be diagnosed by DRS using the second-derivative values at a lipid absorption peak of 1204 nm and by DRS using the first-derivative values at 570 nm and at 550 nm, respectively. Although further study is needed, the results suggest the usefulness of our DRS method for diagnosis of NASH.

Supplementary data to this article can be found online at https://doi.org/10.1016/j.sopen.2021.07.002.

Author Contribution

Yasuhiro Takihata: Investigation, Data curation, Formal analysis, Validation, Writing – original draft. Satoko Kawauchi: Resources, Methodology, Data curation, Validation, Writing – original draft. Sho Ogata: Formal analysis, Investigation, Writing – review & editing. Izumi Nishidate: Methodology, Validation. Shunichi Sato: Conceptualization, Writing – review & editing, Supervision. Junji Yamamoto: Conceptualization, Project administration, Funding acquisition, Writing – review & editing. Yoji Kishi: Project administration, Writing – review & editing.

Conflict of Interest

The authors report no proprietary or commercial interest in any product mentioned or concept discussed in this article.

Funding Source

This work was supported by Grant-in-Aid for Scientific Research (C) from the Japan Society for the Promotion of Science (grant numbers 24592016 and 16K10585).

References

[1] Ahmed A, Wong RJ, Harrison SA. Nonalcoholic fatty liver disease review: diagnosis, treatment, and outcomes. Clin Gastroenterol Hepatol. 2015;13(12):2062–70.
[2] Tapper EB, Lok AS. Use of liver imaging and biopsy in clinical practice. N Engl J Med. 2017;377(8):756–68.
[3] Vishwanath K, Chang K, Klein D, et al. Portable, fiber-based, diffuse reflection spectroscopy (DRS) systems for estimating tissue optical properties. Appl Spectrosc. 2011;65(2):206–15.
[4] Fabila-Bustos DA, Arroyo-Camarena UD, López-Vancell MD, et al. Diffuse reflectance spectroscopy as a possible tool to complement liver biopsy for grading hepatic fibrosis in paraffin-preserved human liver specimens. Appl Spectrosc. 2014;68(12):1357–64.
[5] Bydlon TM, Nachabé R, Ramanujam N, Sterenborg HJ, Hendriks BH. Chromophore based analyses of steady-state diffuse reflectance spectroscopy: current status and perspectives for clinical adoption. J Biophotonics. 2015;8(1–2):9–24.
[6] Evers DJ, Westerkamp AC, Spliethoff JW, et al. Diffuse reflectance spectroscopy: toward real-time quantification of steatosis in liver. Transpl Int. 2015;28(4):465–74.
[7] Nilsson JH, Reistad N, Brange H, Öberg CF, Sturesson C. Diffuse reflectance spectroscopy for surface measurement of liver pathology. Eur Surg Res. 2017;58(1–2):40–50.
[8] Fujii M, Shibazaki Y, Wakamatsu K, et al. A murine model for non-alcoholic steatohepatitis showing evidence of association between diabetes and hepatocellular carcinoma. Med Mol Morphol. 2013;46(3):141–52.
[9] Liang W, Menke AL, Driessen A, et al. Establishment of a general NAFLD scoring system for rodent models and comparison to human liver pathology. PLoS One. 2014;9(12):e115922.
[10] O'Haver TC. Potential clinical applications of derivative and wave-length-modulation spectrometry. Clin Chem. 1979;25:1548–53.
[11] Merrick MF, Pardue HL. Evaluation of absorption and first- and second-derivative spectra for simultaneous quantification of bilirubin and hemoglobin. Clin Chem. 1986;32(4):598–602.
[12] Nachabé R, Evers DJ, Hendriks BH, et al. Diagnosis of breast cancer using diffuse optical spectroscopy from 500 to 1600 nm: comparison of classification methods. J Biomed Opt. 2011;16(8):087010.
[13] Palmer KF, Williams D. Optical properties of water in the near infrared. J Opt Soc Am. 1974;64:1107–10.
[14] Michels R, Foschum F, Kienle A. Optical properties of fat emulsions. Opt Express. 2008;16(8):5907–25.
[15] Lilledahl MB, Haugen OA, Barkost M, Svaasand LO. Reflection spectroscopy of atherosclerotic plaque. J Biomed Opt. 2006;11(2):021005.
[16] Westerkamp AC, Pully VV, Karimian G, et al. Diffuse reflectance spectroscopy accurately quantifies various degrees of liver steatosis in murine models of fatty liver disease. J Transl Med. 2015;13:309.
[17] Arista Romeu EJ, Escobedo G, Campos-Espinosa A, et al. Diffuse reflectance spectroscopy accurately discriminates early and advanced grades of fatty liver in mice. J Biomed Opt. 2018;23(11):1–8.
[18] Reistad N, Nilsson JH, Bergenfeldt M, Rissler P, Sturesson C. Intraoperative liver steatosis characterization using diffuse reflectance spectroscopy. HPB. 2019;21:175–80.
[19] Campbell EL, Bruyninckx WJ, Kelly CJ, et al. Transmigrating neutrophils shape the mucosal microenvironment through localized oxygen depletion to influence resolution of inflammation. Immunity. 2014;40:66–77.
[20] Castera L, Forns X, Alberti A. Non-invasive evaluation of liver fibrosis using transient elastography. J Hepatol. 2008;48(5):835–47.
[21] Venkatesh SK, Wells ML, Miller FH, et al. Magnetic resonance elastography: beyond liver fibrosis-a case-based pictorial review. Abdom Radiol (NY). 2018;43(7):1590–611.
[22] Siddiqui MS, Vuppalanchi R, Van Natta ML, et al. Vibration-controlled transient elastography to assess fibrosis and steatosis in patients with nonalcoholic fatty liver disease. Clin Gastroenterol Hepatol. 2019;17(1):156–163.e2.
[23] Balakrishnan M, Loomba R. The role of noninvasive tests for differentiating NASH from NAFL and diagnosing advanced fibrosis among patients with NAFLD. J Clin Gastroenterol. 2020;54(2):107–13.
[24] Allen AM, Shah VH, Therneau TM, et al. The role of three-dimensional magnetic resonance elastography in the diagnosis of nonalcoholic steatohepatitis in obese patients undergoing bariatric surgery. Hepatology. 2020;71(2):510–21.
[25] Akter S, Maejima S, Kawauchi S, et al. Evaluation of light scattering and absorption properties of in vivo rat liver using a single-reflectance fiber probe during preischemia, ischemia-reperfusion, and postmortem. J Biomed Opt. 2015;20(7):076010.
[26] Serviddio G, Sastre J, Bellanti F, Viña J, Vendemiale G, Altomare E. Mitochondrial involvement in non-alcoholic steatohepatitis. Mol Asp Med. 2008;29:22–35.
[27] Stratonnikov AA, Loschenov VB. Evaluation of blood oxygen saturation in vivo from diffuse reflectance spectra. J Biomed Opt. 2001;6:457–67.
[28] Mesradi M, Genoux A, Cuplov V, Haidar DA, Jan S, Buvat I, et al. Experimental and analytical comparative study of optical coefficient of fresh and frozen rat tissues. J Biomed Opt. 2013;18(11):117010.
[29] Roggan A, Dorschel K, Minet O, Wolff D, Muller G. The optical properties of biological tissue in the near infrared wavelength range—review and measurements. In: Muller G, Roggan A, editors. Laser-induced interstitial thermotherapy. Bellingham, WA: SPIE; 1995. p. 10–44.
[30] Saito K, Uebanso T, Maekawa K, et al. Characterization of hepatic lipid profiles in a mouse model with nonalcoholic steatohepatitis and subsequent fibrosis. Sci Rep. 2015;5:12466.

[31] Dow M, Pyke RM, Tsui BY, et al. Integrative genomic analysis of mouse and human hepatocellular carcinoma. Proc Natl Acad Sci U S A. 2018;115(42):E9879–88.
[32] Chau M, Li Y, Roqueta-Rivera M, et al. Characterization of EDP-305, a highly potent and selective farnesoid X receptor agonist, for the treatment of non-alcoholic steatohepatitis. Int J Gastroenterol. 2019;3(1):4–16.
[33] Lefebvre E, Moyle G, Reshef R, et al. Antifibrotic effects of the dual CCR2/CCR5 antagonist cenicriviroc in animal models of liver and kidney fibrosis. PLoS One. 2016;11(6):e0158156.
[34] Traber PG, Zomer E. Therapy of experimental NASH and fibrosis with galectin inhibitors. PLoS One. 2013;8(12):e83481.
[35] Kleiner DE, Brunt EM, Van Natta M, et al. Design and validation of a histological scoring system for nonalcoholic fatty liver disease. Hepatology. 2005;41(6):1313–21.
[36] Kawauchi S, Sato S, Ooigawa H, Nawashiro H, Ishihara M, Kikuchi M. Simultaneous measurement of changes in light absorption due to the reduction of cytochrome c oxidase and light scattering in rat brains during loss of tissue viability. Appl Opt. 2008;47(22):4164–76.